Appendix

Let us consider an alternating bimetallic chain:

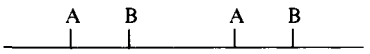

with S_A and S_B local spins, g_A and g_B local g factors, and $J_{AB}(1 + \alpha)$ and $J_{AB}(1 - \alpha)$ interaction parameters between nearest neighbors. S_A is treated as a classical spin and S_B as a quantum spin. One puts

$$J = J_{AB}[S_A(S_A + 1)]^{1/2} \qquad G = g_A[S_A(S_A + 1)]^{1/2}$$

$$g = g_B \qquad s = S_B \qquad x = J/kT$$

The molar magnetic susceptibility is then given by

$$\chi_M = (N\beta^2/3kT)\{g^2[s(s + 1)(1 - P) + 2QR] + 2gG(Q + R) + G^2(1 + P)\}/(1 - P)$$

with

$$P = A_1/A_0$$

$$Q = x[(1 + \alpha)B_0 + (1 - \alpha)B_1]/A_0$$

$$R = x[(1 - \alpha)B_0 + (1 + \alpha)B_1]/A_0$$

and

$$A_0 = (2\pi/\Lambda^2)\sum_{\sigma=-s}^{+s}\sum_{\epsilon=\pm}[\epsilon \exp(\sigma\lambda_\epsilon)/\sigma^2](\sigma\lambda_\epsilon - 1)$$

$$A_1 = (\pi/\Lambda^4)\sum_{\sigma=-s}^{s}\sum_{\epsilon=\pm}[\epsilon \exp(\sigma\lambda_\epsilon)/\sigma^4] \times [\sigma^3\lambda_\epsilon^3 - 3\sigma^2\lambda_\epsilon^2 + (6 - \sigma^2\lambda^2)\sigma\lambda_\epsilon + \sigma^2\lambda^2 - 6]$$

$$B_0 = (2\pi/\Lambda^2)\sum_{\sigma=-s}^{s}\sum_{\epsilon=\pm}\epsilon \exp(\sigma\lambda_\epsilon)$$

$$B_1 = (\pi/\Lambda^4)\sum_{\sigma=-s}^{s}\sum_{\epsilon=\pm}\epsilon \exp(\sigma\lambda_\epsilon)/\sigma^2][\sigma^2\lambda_\epsilon^2 - 2\sigma\lambda_\epsilon + 2 - \sigma^2\lambda^2]$$

λ_+, λ_-, λ^2, and Λ^2 are defined as

$$\lambda_+ = -2x \qquad \lambda_- = \alpha\lambda_+ \qquad \lambda^2 = 2x^2(1 + \alpha^2)$$

$$\Lambda^2 = x^2(1 - \alpha^2)$$

Supplementary Material Available: Tables SVII–SIX giving anisotropic thermal parameters of non-hydrogen atoms, coordinates of hydrogen atoms, and hydrogen bonds for NiCu, Figure S13 giving the experimental and calculated data for the first shell of neighbors at the copper edge, and Figure S14 giving the same information at the manganese edge (5 pages). Ordering information is given on any current masthead page.

Crystal, Molecular Structure, and Magnetic Properties of Bis(tetra-*n*-butylammonium)bis(4-(dicyanomethylene)-1,2-dimercaptocyclopent-1-ene-3,5-dionato-*S*,*S*′)cuprate(II), $[n\text{-}Bu_4N]_2[Cu(dcmdtcroc)_2]$: A Dimer with Weak Ferromagnetic Coupling

N. Venkatalakshmi,[1a] Babu Varghese,[1a] S. Lalitha,[1a] Raymond F. X. Williams,[1b] and P. T. Manoharan*[1a]

Contribution from the Department of Chemistry, Indian Institute of Technology, Madras-600036, India, and Department of Chemistry, Howard University, Washington, D.C. 20059.
Received April 8, 1988

Abstract: An extended dithiolene complex $(n\text{-}Bu_4N)Cu(dcmdtcroc)_2$ has been prepared and characterized by X-ray diffraction and magnetic studies. The crystal structure reveals the anion to be nonplanar and the dihedral angle between the two chelate planes to be 36.76°. The compound crystalizes in the space group *Pbca* with eight molecules per unit cell. The structural parameters are a = 18.087 (7) Å, b = 32.325 (9) Å, c = 18.236 (7) Å, with the intradimer Cu–Cu distance being 4.88 Å. The magnetic susceptibility measurements fitted to the Bleaney–Bower's expression and corrected for molecular field corrections yielded an intradimer ferromagnetic coupling ($2J$ = 12 cm^{-1}) and a very weak interdimer antiferromagnetic coupling (J' = −0.04 cm^{-1}). The powder EPR spectra observed, consistent with the structure and susceptibility findings, show well-resolved triplet spectra at room temperature and a considerable increase in intensity as the temperature is lowered. The spin Hamiltonian parameters have been derived not only from angular variation EPR study of single crystal but also from the computer simulation of polycrystalline EPR spectra at two different frequencies.

The dithiolene complexes of transition-metal ions, $[M(S_2C_2R_2)_2]^{n-}$, where R = H, CN, CF_3, etc. and M = Ni, Cu, Pd, etc., exhibit low-dimensional cooperative phenomena,[2] columnar crystallographic packing,[3] and interesting magnetic properties.[4-8] The variety in stacking and magnetic properties of these metal dithiolene complexes is made possible by their ability to form grossly planar structures irrespective of the metal ion or their oxidation state. Large delocalization of the highest occupied molecular orbitals of π-symmetry is one among the many reasons that promotes columnar stacking, which in turn is responsible for their interesting magnetic properties. In addition, their ability to undergo reversible electron-transfer reactions to yield stable species promotes the formation of donor–acceptor complexes with a variety of organic-based cations. Hence, these systems have

(1) (a) Indian Institute of Technology, Madras, India. (b) Howard University Washington, D. C.

(2) Keller, H. J. *Low Dimensional Cooperative Phenomena*; Plenum: New York, 1975.

(3) Manoharan, P. T.; Noordik, J. H.; de Boer, E.; Keijzers, C. P. *J. Chem. Phys.* **1981**, *74*, 1980–1989.

(4) Kuppusamy, P.; Ramakrishna, B. L.; Manoharan, P. T. *Proc. Indian Acad. Sci.* **1984**, *93*, 977-1001.

(5) Plumlee, K. W.; Hoffmann, B. M.; Ibers, J. A.; Soos, Z. G. *J. Chem. Phys.* **1975**, *63*, 1926–1942.

(6) Plumlee, K. W.; Hoffmann, B. M.; Ratajack, M. T.; Kannewurf, C. R. *Solid State Commun.* **1974**, *15*, 1651–1654.

(7) Isett, L. C.; Rosso, D. M.; Bottger, G. L. *Phys. Rev.* **1980**, *B22*, 4739–4743.

(8) Ramakrishna, B. L.; Manoharan, P. T. *Inorg. Chem.* **1983**, *22*, 2113–2123.

0002-7863/89/1511-5748$01.50/0

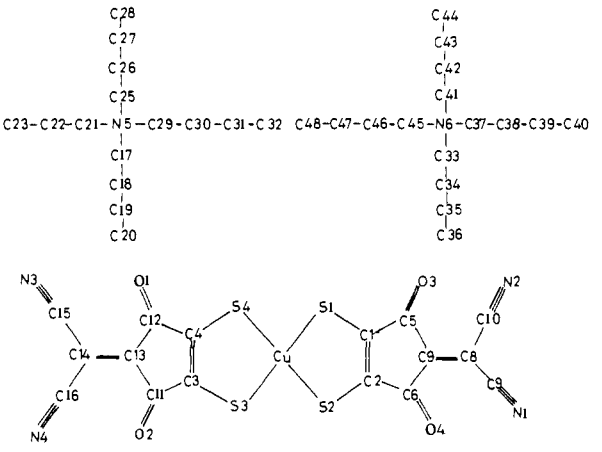

Figure 1. Structural formula $(n\text{-Bu}_4\text{N})_2\text{Cu(dcmdtcroc)}_2$.

attracted the attention of a large group in the fields of X-ray crystallography, magnetic susceptibility, and electron paramagnetic resonance spectroscopy in an attempt to get an insight into the cooperative magnetic phenomena present in them.

Though the planarity of the metal dithiolene anions has been a general feature for most of these systems, thus far, there have been only two reports exhibiting nonplanarity in crystals containing bis(maleonitriledithiolato)cuprate(II), $[Cu(mnt)_2]^{2-}$, anion. Nonplanarity of the complex ions has been observed in the crystal, namely, $(MB^+)_2Cu(mnt)_2\cdot(CH_3)_2CO$ where MB^+ is the methylene blue cation.[9] In this complex the $[Cu(mnt)_2]^{2-}$ anions are paired with a metal–metal distance of 7.115 Å, and the anions have approximately D_2 symmetry with a dihedral angle of 47.4° between the planes of the ligands. The crystal and molecular structure of $(NMe_4)_2Cu(mnt)_2$ reveals the presence of the anion having a D_2 symmetry with an angle of 41.14 (1)° between the normals to the chelate planes, the anions being well separated from each other with the closest Cu–Cu distance of 7.811 Å, while the metal atoms are noncollinear along the stack axis.[10]

In this paper, we report the crystal structure and magnetic properties of another such nonplanar anion, namely, that of bis(tetrabutylammonium)bis(dithiodicyanomethanecroconato)-cuprate(II), $[(n\text{-Bu}_4\text{N})_2\text{Cu(dcmdtcroc)}_2]$, which in many respects is distinctly different from the earlier reported nonplanar dithiolene complexes. The structural formula of the complex is shown in Figure 1. In these crystals, the anions are more dimeric in nature than in the other two systems, and the intradimer metal atoms are separated by a distance of 4.88 Å as compared to more than 7.0 Å in the other two nonplanar dithiolene complexes. Furthermore, the two nonplanar dithiolene components of the dimer are almost one above the other and related by a center of symmetry, and the dihedral angle between the chelate planes is 36.76°. The bulk susceptibility and electron paramagnetic resonance measurements on the present compound agrees fully with the above-mentioned differences. These measurements reveal a ferromagnetic exchange coupling within the dimer and a very weak antiferromagnetic exchange coupling between dimers. Our EPR investigations in pure crystals of these complexes reveal the presence of triplets whose intensities increase enormously on lowering the temperature.

Experimental Section

(I) Preparation of $(n\text{-Bu}_4\text{N})_2\text{Cu(dcmdtcroc)}_2$. The potassium salt of 1,2-dimercaptocyclopent-1-ene-3,4,5-trione [potassium dithiocroconate, K_2(dtcroc)] was prepared by a procedure described elsewhere.[11] Other chemicals were of reagent grade.

A. $(n\text{-Bu}_4\text{N})_2\text{Cu(dtcroc)}_2$. A solution of 1.05 g of $^{63}CuSO_4\cdot5H_2O$ (4.2×10^{-3} mol) in 15 mL of water was added slowly to a warm (50 °C) stirred solution containing 2.67 g of $K_2C_5O_3S_2\cdot2H_2O$ (9.3×10^{-3} mol) in 100 mL of water. The intense reddish brown solution developed a more intense dark brown coloration. Addition of 6.0 g of n-Bu_4NBr (18.6×10^{-3} mol) to the stirred solution caused formation of dark brown precipitate suspended in a red-brown solution. After stirring for 15 min at room temperature and for another 15 min in an ice bath, the mixture was filtered, washed with three 100-mL portions of isopropyl alcohol and two 20-mL portions of petroleum ether, and then air dried. The crude material (4.1 g) was recrystallized from a mixture of hot acetone and isopropyl alcohol in a manner described in literature[11] to yield 3.58 g of $(n\text{-Bu}_4\text{N})_2\text{Cu(dtcroc)}_2$ (4.0×10^{-3} mol) as dark brown plates: mp 138–139 °C. Anal. Found (Calcd): C, 56.76 (56.50); H, 7.63 (8.12); N, 2.90 (3.14); Cu, 6.35 (7.12).

B. $(n\text{-Bu}_4\text{N})_2\text{Cu(dcmdtcroc)}_2$. $(n\text{-Bu}_4\text{N})_2\text{Cu(dtcroc)}_2$ (1.5 g, 1.68×10^{-3} mol) was heated in 20 mL of warm dimethylformamide on a steam bath until dissolved. Maleonitrile (260 mg, 3.36×10^{-3} mol) was added, and the mixture was agitated on the steam bath for 5 min. Hot isopropyl alcohol (60 mL) was added to the reaction mixture, and the vessel was allowed to cool very slowly. The deep blue crystalline solid was separated by decantation, washed with isopropyl alcohol, filtered, and washed with petroleum ether and dried in vacuum at 60 °C. The resulting powder was dissolved in a mixture of acetonitrile and acetone (2:1 v/v), and the solution was evaporated slowly at 20 °C to yield blue black crystals with well-developed faces.

(II) Crystal Structure Determination. A. Collection and Reduction of X-ray Data. A crystal of size $0.45 \times 0.20 \times 0.40$ mm^3 with a plate-like morphology was chosen for study, and three dimensional intensity data were collected at room temperature (23 °C) on an Enraf Nonius CAD-4F single-crystal X-ray diffractometer with graphite monochromated Cu Kα radiation (λ = 1.5418 Å). The unit cell dimensions were determined by using 25 reflections having $80° < 2\theta < 100°$. The space group was determined as *Pbca*. The lattice parameters are a = 18.087 (7) Å, b = 32.325 (9) Å, c = 18.237 (7) Å, Z = 8, V = 10 662 Å^3, D_m = 1.24 (1) g cm^{-3}, D_c = 1.237 g cm^{-3}, μ = 21.45 cm^{-1}. Intensity data were collected by ω-2θ scans at variable scan speed with maximum scan time of 1 min per reflection. Intensities of two control reflections chosen from two different zones of reciprocal space were monitored once every 1 h to ensure the stability of the crystal in X-ray beam. A total of 10953 unique reflections were collected with a maximum Bragg angle of 70 out of which 5784 reflections satisfying the condition $I > 3\sigma(I)$ were chosen for structure solution. The intensity of these reflections were corrected for Lorentz, polarization, and absorption effects. The crystal used for data collection had an approximate morphology of a parellelopiped. The Miller indices of the faces were (0 1 0), (1 0 1), (1 0 −1), (0 −1 0), (−1 0 −1), and (−1 0 1). Since the crystal has a linear absorption coefficient of 21.45 cm^{-1}, numerical absorption correction was done using SHELX-76 computer program.[12] The maximum and minimum transmission factors were 0.4051 and 0.2787, respectively.

B. Solution and Refinement of the Structure. The direct method of structure solution in the SHELX-76[12] computer program was used to locate the positions of the copper atom and four sulfur atoms. Successive Fourier synthesis yielded all the remaining non-hydrogen atoms. The structure was refined by using full-matrix least-squares technique with isotropic thermal parameters for individual atoms. After the full convergence of the isotropic refinement, the atoms were assigned anisotropic thermal parameters and further refined by full-matrix least-squares technique. Difference Fourier map synthesized after full convergence of least-squares refinement showed 62 out of 72 hydrogen atoms at chemically meaningful positions. The positions of the hydrogen atoms from difference map were verified also by fixing all hydrogen atoms geometrically. The fixed hydrogen atoms were given an isotropic temperature factor of 0.05 A^2 which is nearly equivalent to the overall temperature factor of the crystal. The hydrogen atoms were not refined. The final R factor obtained is 0.0622 with unit weights. The weighted refinement of the structure with $w = ((\sigma(R))^2 + 0.0363F^2)^{-1}$ increased the R factor to 0.081 with no significant improvements in bond lengths. Hence, the results of refinement with unit weights were taken for structural data.

(III) Magnetization Measurements. The magnetic susceptibility of powdered $(n\text{-Bu}_4\text{N})_2\text{Cu(dcmdtcroc)}_2$ was measured in a Princeton Applied Research Model 155 vibrating sample magnetometer. The instrument was calibrated against the saturation moment of nickel metal. A Janis continuous flow cryostat introduced between the pickup coils allowed temperature regulation in the range 1.8–300 K; a carbon resistor thermometer was used to measure the temperature to an accuracy within ±1 K above 50 K and ±0.1 K below 50 K. The susceptibility measurements were made from 298 K down to 3.23 K. All measurements were done at a constant homogeneous field of 0.6 T. There was no

(9) Snaathorst, D.; Doesburg, H. M.; Perenboom, J. A. A. J.; Keijzers, C. P. *Inorg. Chem.* **1981**, *20*, 2526–2532.
(10) Mahadevan, C.; Seshasayee, M. *J. Cryst. Spect. Res.* **1984**, *14*, 213–224.
(11) Seitz, G.; Mann, K.; Matsch, R. *Arch. Pharm.* **1975**, *308*, 792–795.
(12) Sheldrick, G. M. SHELX-76 *Program for Crystal Structure Determination*; University of Cambridge, England, 1976.

Table I. Fractional Coordinates ($\times 10^4$) for Non-Hydrogen Atoms[a]

atom	x	y	z	atom	x	y	z	atom	x	y	z
Cu	4933 (0)	484 (0)	6025 (1)	N(1)	4558 (4)	2232 (3)	2759 (6)	C(29)	1866 (4)	2148 (2)	1045 (4)
S(1)	3861 (1)	850 (1)	5948 (1)	N(2)	2469 (4)	2263 (2)	3823 (5)	C(30)	2238 (5)	2076 (3)	314 (5)
S(2)	5488 (1)	861 (1)	8122 (1)	N(3)	5764 (6)	−1115 (4)	9475 (5)	C(31)	2305 (6)	1606 (3)	198 (6)
S(3)	5669 (1)	−78 (1)	5828 (1)	N(4)	6993 (4)	−1611 (2)	7731 (4)	C(32)	2671 (7)	1499 (4)	−547 (7)
S(4)	4824 (1)	303 (1)	7216 (1)	O(1)	5158 (3)	−308 (2)	8531 (3)	N(6)	1753 (3)	288 (2)	4636 (3)
C(1)	4073 (3)	1154 (2)	5224 (4)	O(2)	6476 (2)	−871 (1)	6554 (3)	C(33)	1022 (3)	317 (2)	5046 (4)
C(2)	4766 (3)	1159 (2)	4884 (4)	O(3)	2930 (3)	1522 (2)	5030 (3)	C(34)	962 (4)	687 (3)	5562 (4)
C(3)	5661 (3)	−285 (2)	6665 (3)	O(4)	5275 (3)	1556 (2)	3890 (4)	C(35)	181 (5)	694 (3)	5892 (6)
C(4)	5259 (3)	−123 (2)	7260 (4)	N(5)	1735 (3)	2597 (2)	1247 (3)	C(36)	38 (7)	1084 (3)	6357 (7)
C(5)	3575 (4)	1447 (2)	4879 (4)	C(17)	2447 (4)	2845 (2)	1294 (4)	C(37)	1948 (4)	695 (2)	4262 (4)
C(6)	4757 (4)	1461 (2)	4297 (4)	C(18)	3007 (4)	2691 (3)	1846 (5)	C(38)	1356 (4)	852 (2)	3727 (4)
C(7)	3995 (4)	1643 (2)	4284 (4)	C(19)	3613 (5)	3023 (3)	1929 (6)	C(39)	1585 (5)	1284 (3)	3507 (6)
C(8)	3755 (4)	1927 (2)	3810 (5)	C(20)	3423 (9)	3366 (5)	2412 (8)	C(40)	991 (7)	1457 (4)	2933 (7)
C(9)	4221 (4)	2087 (3)	3226 (5)	C(21)	1338 (4)	2587 (2)	1985 (4)	C(41)	1674 (4)	−64 (2)	4094 (4)
C(10)	3031 (5)	2104 (2)	3830 (5)	C(22)	1122 (5)	2993 (3)	2297 (5)	C(42)	2350 (4)	−140 (3)	3626 (5)
C(11)	6061 (3)	−656 (2)	6904 (4)	C(23)	862 (5)	2929 (3)	3088 (5)	C(43)	2218 (5)	−497 (3)	3105 (5)
C(12)	5395 (3)	−370 (2)	7918 (4)	C(24)	633 (6)	3331 (4)	3452 (7)	C(44)	2903 (6)	−593 (4)	2640 (6)
C(13)	5876 (3)	−717 (2)	7689 (4)	C(25)	1270 (4)	2833 (2)	665 (4)	C(45)	2397 (3)	210 (2)	5183 (4)
C(14)	6116 (3)	−1028 (2)	8109 (4)	C(26)	541 (4)	2632 (3)	459 (5)	C(46)	2356 (5)	−191 (3)	5612 (5)
C(15)	5920 (5)	−1058 (3)	8878 (5)	C(27)	221 (6)	2866 (4)	−191 (6)	C(47)	3057 (5)	−215 (3)	6075 (4)
C(16)	6612 (4)	−1346 (2)	7876 (4)	C(28)	−540 (7)	2690 (5)	−398 (8)	C(48)	3083 (6)	−589 (3)	6561 (6)

[a] Standard deviation in last digit is given in parentheses.

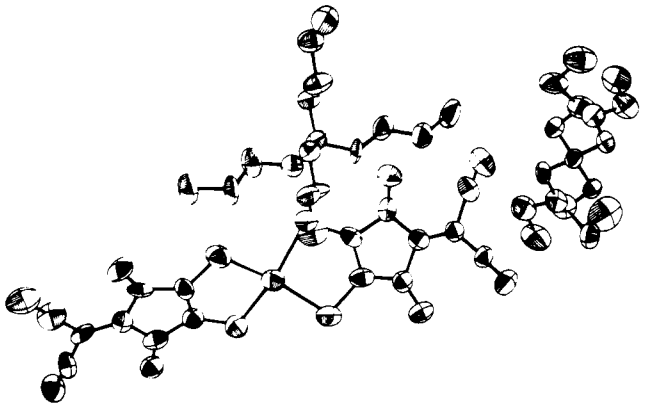

Figure 2. An ORTEP plot of the molecule $(n\text{-}Bu_4N)_2Cu(dcmdtcroc)_2$.

saturation of magnetization at this field.

(iv) **EPR Measurements.** Powder and single-crystal EPR spectral measurements were made with an E-112 Varian instrument at X- and Q-band frequencies at 100 kHz modulation. 2,2-Di(4-*tert*-octylphenyl)-1-picrylhydrazyl (DPPH) was used as a frequency marker. The X-band spectra were recorded on Varian E4 instrument. By using a CTI-Cryogenics Cryodyne Cryocooler, it was possible to reach 20 K. The crystal was of flat rhombic shape with the flat side corresponding to the *ac* plane and the two diagonals, the *a* and *c* axes, respectively. The crystals with good morphology were rotated in a Varian E-112 EPR spectrometer at Q-band fields, with the magnetic field B being swept on the crystallographic *ab*, *bc*, and *ac* planes.

Results and Discussion

(i) **Crystal Structure.** An ORTEP plot of the molecule is shown in Figure 2. Table I shows the fractional atomic coordinates of non-hydrogen atoms. Table II shows bond distances and bond angles of the anion.[13] All the bond lengths and bond angles are normal within the limits of standard deviations. The double bonds C(1)–C(2) (1.399 Å) and C(3)–C(4) (1.407 Å) are considerably elongated from ideal C=C (1.337 Å) because of their conjugation with C=O groups attached to the five-membered rings. Consequently the single bonds C(1)–C(5) (1.451 Å), C(2)–C(6) (1.447 Å), C(3)–C(11) (1.464 Å), and C(4)–C(12) (1.463 Å) are shortened. The average C–N bond lengths in the cation is 1.525(9) Å, and the average C–N–C bond angle 109.49 (5)°. The average C–C distance in the cation is 1.523 (12) Å, and the average C–C–C bond angle is 110.1 (5)°. Table III shows the equations of the least-square mean planes of the anion along with the deviation of atoms from the mean planes.

A projection of the molecular packing onto *the ab* plane is shown in Figure 3. The cations are represented by circles at the position of the nitrogen atoms. The anions form clear dimers and are seen to pack along two different directions, with the bulky $n\text{-}Bu_4N^+$

Table II. Bond Distances and Bond Angles in $[Cu(dcmdtcroc)_2]^{2-}$[a]

Bond Distances (Å)			
Cu–S(1)	2.276 (2)	C(7)–C(8)	1.336 (10)
Cu–S(2)	2.281 (2)	C(8)–C(10)	1.431 (11)
Cu–S(3)	2.280 (2)	C(5)–O(1)	1.242 (21)
Cu–S(4)	2.281 (2)	C(6)–O(2)	1.170 (20)
S(1)–C(1)	1.690 (7)	C(7)–O(3)	1.219 (21)
S(2)–C(2)	1.679 (6)	C(8)–O(4)	1.204 (22)
S(3)–C(3)	1.669 (7)	C(13)–C(14)	1.336 (9)
S(4)–C(4)	1.684 (7)	C(14)–C(15)	1.451 (12)
C(1)–C(2)	1.399 (7)	C(14)–C(16)	1.429 (10)
C(3)–C(4)	1.407 (9)	C(15)–N(3)	1.139 (13)
C(1)–C(5)	1.457 (9)	C(16)–N(4)	1.131 (10)
C(2)–C(6)	1.447 (10)	C(9)–C(10)	1.329 (23)
C(5)–C(7)	1.468 (10)	C(8)–C(9)	1.451 (12)
C(6)–C(7)	1.499 (10)	C(10)–C(12)	1.433 (24)
C(4)–C(12)	1.463 (10)	C(9)–N(1)	1.147 (13)
C(3)–C(11)	1.464 (9)	C(10)–N(2)	1.137 (11)
Bond Angles (deg)			
S(1)–Cu–S(2)	93.0 (1)	S(2)–Cu–S(3)	93.2 (1)
S(1)–Cu–S(3)	154.3 (1)	S(2)–Cu–S(4)	153.8 (1)
S(1)–Cu–S(4)	92.9 (1)	S(3)–Cu–S(4)	92.4 (1)
Cu–S(1)–C(1)	99.0 (2)	Cu–S(3)–C(3)	99.8 (2)
Cu–S(2)–C(2)	98.7 (2)	Cu–S(4)–C(4)	99.2 (2)
S(2)–C(2)–C(1)	125.1 (5)	S(4)–C(4)–C(3)	124.4 (5)
S(2)–C(2)–C(6)	125.8 (5)	S(4)–C(4)–C(12)	125.6 (5)
S(1)–C(1)–C(5)	125.3 (5)	S(3)–C(3)–C(4)	124.1 (5)
S(1)–C(1)–C(2)	123.9 (5)	S(3)–C(3)–C(11)	126.6 (5)
C(5)–C(1)–C(2)	110.8 (6)	C(3)–C(4)–C(12)	110.0 (6)
C(1)–C(2)–C(6)	109.1 (6)	C(4)–C(3)–C(11)	109.3 (5)
C(1)–C(5)–C(7)	106.3 (5)	C(4)–C(12)–C(13)	106.3 (6)
C(1)–C(5)–O(3)	128.7 (6)	C(4)–C(12)–O(1)	127.3 (6)
C(7)–C(5)–O(3)	125.1 (6)	C(13)–C(12)–O(1)	126.4 (7)
C(2)–C(6)–C(7)	106.6 (6)	C(3)–C(11)–C(13)	106.5 (5)
O(4)–C(6)–C(2)	127.3 (7)	C(3)–C(11)–O(2)	128.4 (6)
C(5)–C(7)–C(8)	127.4 (6)	C(12)–C(13)–C(14)	126.8 (6)
C(6)–C(7)–C(8)	125.4 (7)	C(11)–C(13)–C(14)	125.5 (6)
C(5)–C(7)–C(6)	107.2 (6)	C(12)–C(13)–C(11)	107.7 (5)
C(9)–C(8)–C(10)	114.2 (7)	C(15)–C(14)–C(16)	112.7 (7)
C(7)–C(8)–C(9)	122.9 (7)	C(13)–C(14)–C(15)	121.8 (7)
C(7)–C(8)–C(10)	123.8 (7)	C(13)–C(14)–C(16)	125.4 (7)
N(1)–C(9)–C(8)	175.8 (9)	N(3)–C(15)–C(14)	174.6 (10)
N(2)–C(10)–C(8)	176.1 (9)	N(4)–C(16)–C(14)	176.6 (8)

[a] Standard deviation in last digit is given in parentheses.

(13) Hydrogen positional parameters with isotropic temperature factors, anisotropic temperature factors of non-hydrogen atoms, and a F_o–F_c table are available along with the Supplementary Material.

Table III. Least-Squares Planes of the Anion[a]

plane I		plane II	
atom	deviation (Å × 10³)	atom	deviation (Å × 10³)
Cu	72	Cu	−38
S(1)	−54	S(3)	13
S(2)	−35	S(4)	35
C(1)	−11	C(3)	10
C(2)	−17	C(4)	17
C(5)	16	C(11)	−5
C(6)	−5	C(12)	38
C(7)	33	C(13)	6

[a] Equations: plane I, −0.3145 X, −0.6980 Y, −0.64332 Z = −11.0387; plane II −0.7905 X, −0.5573 Y, −0.2542 Z = −10.6795. X, Y, and Z (in Å coordinates) are measured in the directions a, b, and c deviation of atoms from the planes.

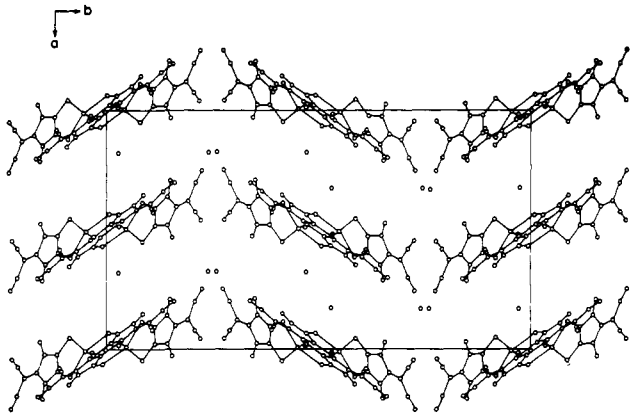

Figure 3. Projection of the packing arrangement of Cu(dcmdtcroc)$_2$ on to ab plane.

cations appearing in pairs. The two molecules in a dimer are related to each other by an inversion symmetry. The Cu–Cu distance within a dimer is 4.883 (1) Å. The closest interpair Cu–Cu distance being 10.538 (1) Å. The distances to the other nearest neighboring Cu atoms are 13.07, 13.40, and 15.73 Å. The nearest distance between the centers of the dimers is 12.86 Å which is half of the diagonal to the ac plane. When we consider the two ligand planes including the metals of a dimer, related to each other by the center of symmetry, they are found almost one above the other, the displacement being 0.13 Å along the length of these anions, and 1.91 Å laterally. The Cu atom of one of the monomer units is closest to the S(1) of the other monomer unit (3.8 Å) within the dimer. The anions are nonplanar, with the dihedral angle between the two ligand planes being 36.76° reducing the symmetry of individual anions to D_2. Such nonplanar geometry around the metal atom in dithiolenes is very rare, the only earlier examples being those of $(MB^+)_2Cu(mnt)_2$ and $(NMe_4)_2Cu(mnt)_2$. The presence of both the cations associated with the single complex anion $[Cu(dcmdtcroc)_2]^{2-}$, in the vicinity of only one of the bidentate ligands (as seen in Figure 2), might have caused a twist around Cu–S bonds and given rise to a torsion potential. This might well be the reason for nonplanarity seen in this compound. Probably, this structure and packing arrangement represents the minimum total energy of the complete system.

(ii) Magnetic Susceptibility. Figure 4 shows a plot of molar susceptibility as a function of temperature in the range 3.2–103 K. No distinct maximum or cutoff is seen in the plot. The experimental data was fitted with Bleaney–Bower's[14] expression for an exchange coupled pair of $S = 1/2$ spins as given by

$$\chi_M = \frac{2N\bar{g}^2\mu_B^2}{kT}[3 + \exp(-2J/kT)]^{-1} \quad (1)$$

where $\bar{g}$, μ_B, and k have the usual meaning. By using the average

(14) Bleaney, B.; Bower, K. D. *Proc. Roy. Soc. London, Sec. A* **1952**, *214*, 451–465.

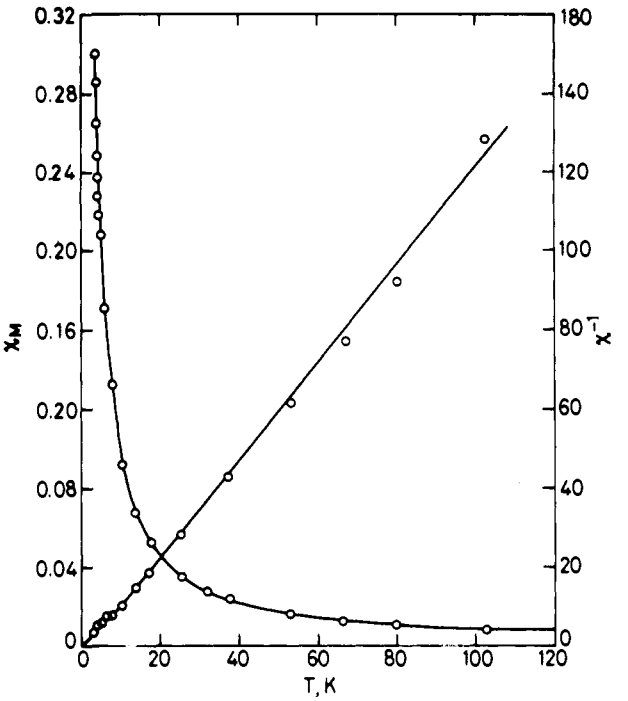

Figure 4. Temperature variation of susceptibility of $(n\text{-}Bu_4N)_2$ Cu(dcmdtcroc)$_2$ at a field of 0.6 T. Open circles represent experrimental values. Solid lines represent the calculated susceptibility based on Bleaney–Bower's equation corrected for molecular fields. Both χ_M vs T and χ_M^{-1} vs T are plotted.

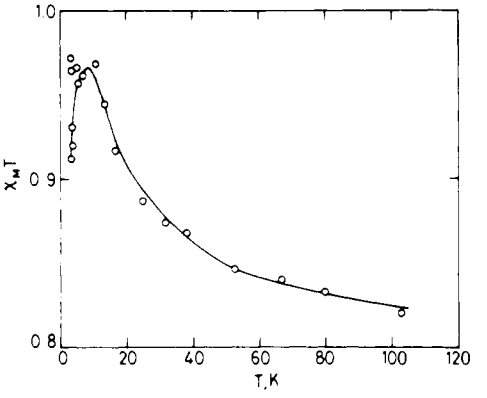

Figure 5. Temperature variation of $\chi_M T$ of $(n\text{-}Bu_4N)_2Cu(dcmdtcroc)_2$. Solid line represents the theoretically calculated susceptibility, while circles indicate the experimental points.

$\bar{g}$ (2.06) from EPR results a least-squares fit was performed by varying the J value to minimize the error function

$$f(\bar{g}, J) = \frac{1}{N}\sum_{i=1}^{n}[\chi_M^{exp}(T_i) - \chi_M^{calcd}(T_i)]^2T_i^2 \quad (2)$$

This led to a $2J$ value of 3.4 cm^{-1} with an error of 5.3%. Because of this low value of J accompanied by a high error, the possibility of interdimer exchange (J') was considered by including a molecular field correction. The corrected susceptibility is given by

$$\chi_M^{corr} = \chi_M/(1 - 2ZJ'\chi_M/N\bar{g}^2\mu_B^2) \quad (3)$$

where χ_M is the simple Heisenberg susceptibility of eq 1, and Z is the number of nearest neighboring spin centers and is found to be 6 from the crystal structure. A least-squares fit, varying both J and J' and minimizing the same error function (eq 2) yielded $2J$ = 12 cm^{-1} and J' = −0.041 cm^{-1} with an average error of 3%. The theoretical susceptibilities calculated by using these values fit very well with the experimental points (Figure 4). This indicates that the two spins are ferromagnetically coupled within

Figure 6. Polycrystalline EPR spectrum of $(n\text{-}Bu_4N)_2Cu(dcmdtcroc)_2$ at X-band frequence: (a) simulated theoretically and (b) experimental spectrum.

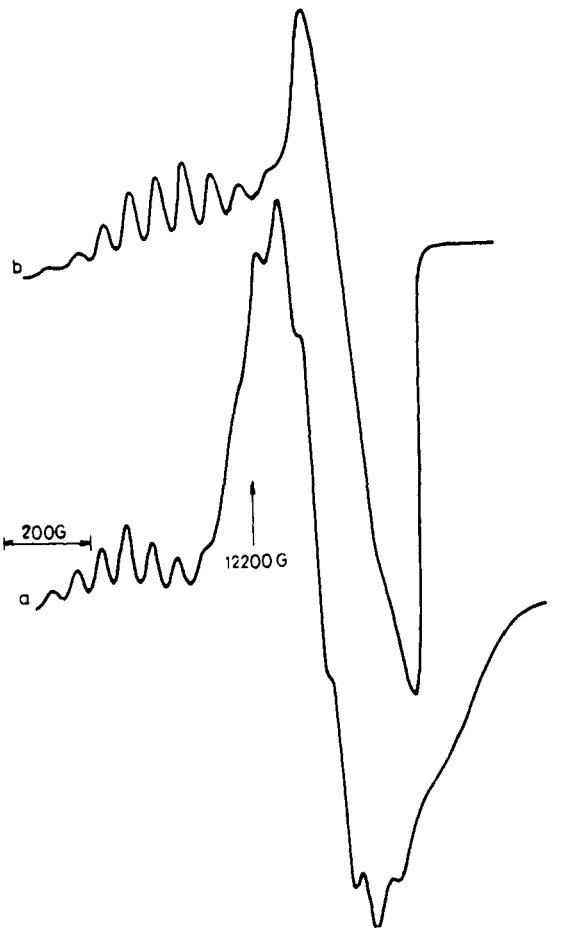

Figure 7. Polycrystalline EPR spectrum of $(n\text{-}Bu_4N)_2Cu(dcmdtcroc)_2$ at Q-band frequency: (a) simulated theoretically and (b) experimental spectrum.

the dimer, while an antiferromagnetic coupling exists between the dimers.

The plot of $\chi_M T$ vs T (Figure 5) shows an increase off susceptibility with a decrease in temperature down to 10 K, below which the points are scattered. The resultant curve is an indication of a strong ferromagnetic interaction within the dimer. At temperatures lower than 10 K, triplet states are highly populated and consequently will give rise to strong triplet–triplet interaction. As already seen from the susceptibility fit using eq 3, the interdimer interaction is antiferromagnetic, while the intradimer interaction is ferromagnetic.

(iii) Polycrystalline Electron Paramagnetic Resonance Spectra. The polycrystalline EPR spectra at room temperature, at both X- and Q-band fields, show well-resolved spectra due to ground triplet state indicating the presence of a ferromagnetically coupled dimer (Figures 6 and 7). The **D** values observed in these are very small, and consequently we are unable to observe the half field transition ($\Delta M_s = \pm 2$), as its intensity is proportional to $\mathbf{D}^2$ for an axially symmetric system. The polycrystalline EPR spectra can be theoretically simulated as described by Smith and Pilbrow.[15] The program GNDIMER[15] was used for the EPR spectral simulation. There appears to be some mismatch between the experimental and computer-simulated curves (Figure 6 and 7) due to the limitations on the speed required for computation. However, the fits are good when judged by how well various peaks match, rather than superposition of the calculated with experimental spectra. The best fit with the experimental curve in our case is observed by treating the system as axial with the values $\mathbf{g}_\perp = 2.03$, $\mathbf{g}_\parallel = 2.09$, $\mathbf{A}_\perp = 30 \times 10^{-4}$ cm^{-1}, $\mathbf{A}_\parallel = 120 \times 10^{-4}$ cm^{-1}, $2J = 12$ cm^{-1}, and the internuclear distance $r = 5.0$ Å. The matching is better for the X-band spectra than that of the Q-band. It is gratifying to note that the above values agree very well with the sueceptibility result ($2J = 12$ cm^{-1}) and crystallographic result ($r = 4.88$ Å). The **g** and **A** tensor values are also in close agreement to those evaluated from single-crystal EPR studies as discussed later in this paper.

The polycrystalline EPR spectrum as a function of temperature reveals some interesting features. (i) The **D** tensor remains axially symmetric throughout the temperature range. (ii) The integrated intensity increases on lowering the temperature (Figure 8) confirming the ferromagnetic coupling between the dimerically coupling anions. (iii) A slight increase in the intensity of the low field lines (due to the $\mathbf{D}_{zz}$ component) at lower temperatures indicates the sign of **D** to be negative. (iv) There is an apparent increase of the **D** value on cooling from **D** = 102 G at 300 K to **D** = 114 G at 40 K. This may be due to contraction of the crystal leading to either a slight increase in dihedral angle or a decrease in the intercopper distance.

(iv) Exchange Coupling Constant Derived from EPR Intensity. The crystal $(n\text{-}Bu_4N)_2Cu(dcmdtcroc)_2$ is an excellent example of the presence of intradimer coupling and interdimer coupling. Neglecting the nuclear spins, a system of such coupled triplet centers in zero magnetic field can be generally described by the Hamiltonian[16]

$$\mathcal{H} = \mathcal{H}_D + \mathcal{H}_O \qquad (4)$$

where $\mathcal{H}_D$ is the magnetic dipolar interaction between the four unpaired electrons and $\mathcal{H}_O$ the electrostatic interaction. We

(15) Smith, T. D.; Pilbrow, J. R. *Coord. Chem. Rev.* **1974**, *13*, 173–282.

(16) (a) Benk, H.; Sixl, H. *Mol. Phys.* **1981**, *42*, 779–783. (b) Kollmar, C.; Sixl, H.; Benk, H.; Denner, V.; Mahler, G.; *Chem. Phys. Lett.* **1982**, *87*, 266. (c) Snaathorst, D.; Keijzers, C. P. *Mol. Phys.* **1984**, *51*, 509.

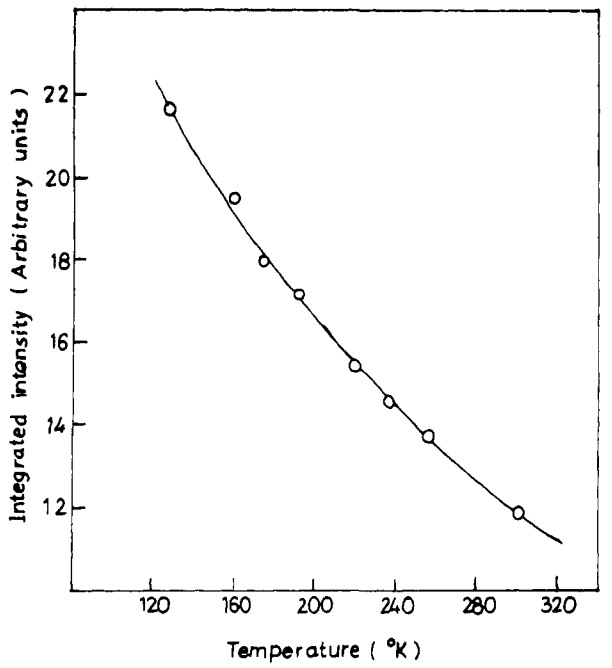

Figure 8. Temperature variation of integrated EPR intensity of $(n\text{-}Bu_4N)_2Cu(dcmdtcroc)_2$ at X-band frequency.

Table IV. Relative Population in TT, (TS, ST) and SS Levels As a Function of Temperature

temp (K)	TT	TS, ST	SS
25	0.4437	0.4448	0.1115
100	0.2949	0.4963	0.2088
200	0.2720	0.4991	0.2285
300	0.2646	0.4996	0.2358
400	0.2609	0.4998	0.2393

represent the two dimers as I and II, each consisting of the monomers A and B; I contains electrons 1 and 2, while II contains the electrons 3 and 4. With these notations the two electron terms of the electrostatic interactions are presented by the effective spin Hamiltonian[16]

$$\mathcal{H}_O = \mathcal{H}_{O,intra} + \mathcal{H}_{O,inter}$$
$$= -2J_{intra}(\vec{S}_1\cdot\vec{S}_2 + \vec{S}_3\cdot\vec{S}_4) - 2J_{inter}(\vec{S}_1 + \vec{S}_2)\cdot(\vec{S}_3 + \vec{S}_4) \quad (5)$$

The $\mathcal{H}_{O,intra}$ is known from the susceptibility measurements and is seen to be the most dominant interaction. We also have an idea of J_{inter} from susceptibility measurements though the accuracy could be less. Since the dimer has been proved to be ferromagnetic from susceptibility experiments, the above Hamiltonian results in a triplet ground state and a singlet excited state for each individual dimer.

In only $\mathcal{H}_{O,intra}$ is taken into consideration, then, in a system of two dimers like ours, the energy level diagram shown in Figure 9A holds. The ground state has the triplet–triplet interaction, represented as TT, and the first excited state gives the isolated triplet, i.e., triplet(I)–singlet(II) (TS) and singlet(I)–triplet(II) (ST). The other excited state will be single(I)–singlet(II) (SS) and this is EPR inactive. Assuming the J value obtained from susceptibility, the relative Boltzman populations estimated at various temperatures in these three states are given in Table IV. This clearly shows that at room temperature, the population of the isolated triplets will be dominant, with reasonably large contributions from the TS state. Hence, the triplet–triplet lines will also show up in single-crystal EPR spectra.

The energy separation between the single (S), triplet (T), and quintet (Q) states is brought about by the electrostatic interactions among the electrons. Two different exchange integrals are involved in bringing about this resulting separation viz. (i) J_2—the exchange of an electron pair between the two triplets, giving rise to the separation among T, S, and Q and (ii) J_1—which describes the

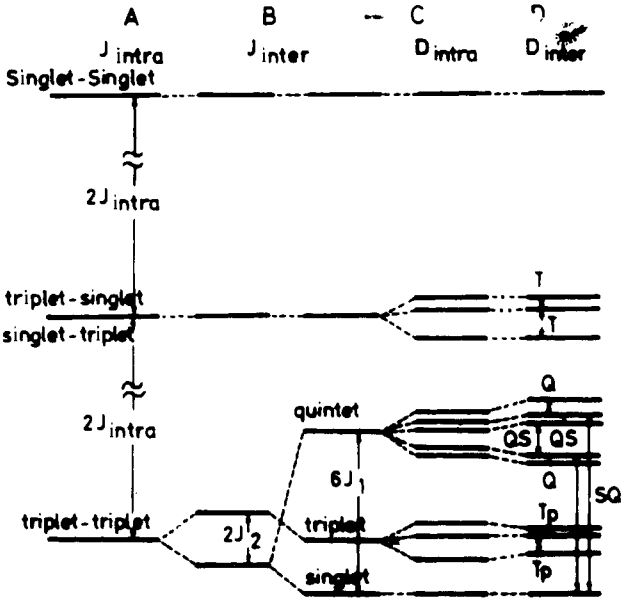

Figure 9. Schematic energy level diagram for a system of two interacting pairs of dimers.

exchange of single electrons and brings about the separation between S and Q. The energy level diagram resulting from these, with an arbitrary J_2/J_1 ratio, is given in Figure 9B. However, one has to remember at this point that both J_1 and J_2 are much smaller than J in magnitude.

The S and Q states are mixed due to the dipolar interaction among the four electrons while the T pair state remains undisturbed due to the difference in symmetry of its wave function from those of S and Q. The dipolar Hamiltonian is given as

$$\mathcal{H}_D = \vec{S}_1\cdot\mathbf{D}_{intra}\cdot\vec{S}_2 + \vec{S}_3\cdot\mathbf{D}_{intra}\cdot\vec{S}_4 + (\vec{S}_1 + \vec{S}_2)\cdot\mathbf{D}_{inter}\cdot(\vec{S}_3 + \vec{S}_4) \quad (6)$$

Making some approximations, viz. (i) assuming orthogonal orbital wave functions and (ii) neglecting the exchange type integrals between dimers which is justified in our case due to large distances between the paramagnetic centers, the ZFS tensors $\mathbf{D}_{intra}$ and $\mathbf{D}_{inter}$ have been described by Snaathorst et al.[10] and Benk and Sixl.[16] The descriptions given in these references reveal that the interdimer dipolar interaction is seen to be an average of the four individual interactions between the electrons in one dimer to those in the other dimer. The inclusion of these interactions leads to the splitting of energy levels as seen in the energy level diagram (Figures 9C and 9D) where the S and Q functions are seen to be mixed. As seen in the figure, the excited state is influenced only by $\mathbf{D}_{intra}$ and not by $\mathbf{D}_{inter}$. The crystal structure shows the interdimer distance to be very large, 10.538 Å, thus justifying the neglect of $\mathbf{D}_{inter}$.

It is a well-known fact that the EPR line intensity is a direct measure of susceptibility of the system under study. This intensity is directly proportional to the differences in population in the various energy levels, between which the transitions take place to give rise to the EPR spectra. In the temperature range $kT >> |J|$ the signal intensity is given as[17]

$$I \propto \frac{1}{Z}\,[\mathrm{Xp}(-E/kT) - \exp(-E + h\nu)/kT] \quad (7)$$

where Z is the partition function, and $h\nu$ is the gap between the two energy levels.

For our system of two interacting dimers, using the energy level scheme as derived earlier, we considered three cases. In all these cases we neglect both $\mathbf{J}_{inter}$ and $\mathbf{D}_{inter}$ as is justified from the suscaptibility and crystallographic results.

Case (a)—An Isolated Dimer. In such a case the first excited state in Figure 9A is considered as the ground state with only one

(17) Harris, E. A.; Owen, J. *Proc. Roy. Soc.* **1965**, *A289*, 122-137.

excited state (SS). The transition giving rise to the EPR spectra is due to the TS state population and the intensity is given as

$$I \propto \frac{1}{Z}\,[1 - \exp(-2\bar{g}\mu_B\vec{B}/kT)] \qquad (8)$$

where

$$Z = 1 + \exp(-2\bar{g}\mu_B\vec{B}/kT) + \exp(-\bar{g}\mu_B\vec{B}/kT) + \exp[-(2J + \bar{g}\mu_B\vec{B})/kT]$$

Since the intensity is a function of temperature, the temperature variation of intensity will permit the evaluation of $2J$. Using the ratio I_T/I_{RT} where I_T and I_{RT} are the integrated EPR intensities at temperature T and room temperature, respectively, one can get rid of the proportionality constant. A least-squares fit gives $2J = -48.45$ cm^{-1}. This value is far different both in magnitude and sign from the experimental values.

Case (b)—Interdimer Interaction. Here the total energy level scheme as shown in Figure 9D is considered. The transition intensity is thus considered to be the sum of the transition due to $\Delta M_s = \pm 1$ both within the TT, TS, and ST states. The intensity is then seen to be

$$I_T \propto \frac{1}{Z}\,[1 + 2\exp(-\bar{g}\mu_B\vec{B}/kT) - 2\exp(-3\bar{g}\mu_B\vec{B}/kT) - \exp(-4\bar{g}\mu_B\vec{B}/kT) + \exp[-(2J + \bar{g}\mu_B\vec{B})/kT] - \exp[-(2J + 3\bar{g}\mu_B\vec{B})/kT] \qquad (9)$$

where

$$Z = 1 + 2\exp(-\bar{g}\mu_B\vec{B}/kT) + 3\exp(-2\bar{g}\mu_B\vec{B}/kT) + 2\exp(-3\bar{g}\mu_B\vec{B}/kT) + \exp(-4\bar{g}\mu_B\vec{B}/kT) + 2\exp(-2J/kt)[\exp(-\bar{g}\mu_B\vec{B}/kT) + \exp(-2\bar{g}\mu_B\vec{B}/kT) + \exp(-3\bar{g}\mu_B\vec{B}/kT)]$$

A least-squares fit as carried out in case (a) with the intensity given as in expression 9 gives a $2J$ value of 25.26 cm^{-1}. The calculated value is now approximately twice the experimental value. Unfortunately this model assumes that all the dimers will have a triplet-triplet interaction, i.e., each and every dimer is coupled to another. However, this is far from the truth, and both an isolated dimer and the interacting dimer should be considered using a statistical approach.

Case (c)—Statistical Consideration of Both Isolated Dimers and Interacting Dimers. In any system of two interacting dimers the probability of two neighboring dimers to be in a triplet state is given by

$$P_{TT} = X^2 \qquad (10)$$

where X is the probability for populating the triplet state in a ferromagnetically coupled dimer, given as

$$X = 3/(3 + \exp(-2J/kT)) \qquad (11)$$

Now the probability for an isolated dimer, i.e., TS or ST state is given as

$$P_{TS} = X(1 - X) \qquad (12)$$

Therefore, the intensity equation now becomes

$$I_T \propto P_{TT}I_{TT} + P_{ST}I_{ST} \qquad (13)$$

where I_{TT} is the intensity given by eq 9 and I_{ST} the intensity as given in eq 8.

Now using the intensity expression given in eq 13 and fitting the intensity ratio I_T/I_{RT}, we arrive at a $2J$ value of 12.4 cm^{-1}, which is indeed very close to the bulk susceptibility result of 12 cm^{-1}. Considering that we have simplified the calculations by neglecting $\mathbf{D}_{inter}$ and $\mathbf{J}_{inter}$, this value of exchange coupling constant as evaluated from EPR intensity study is indeed highly satisfactory.

(v) Single-Crystal EPR Study. To get further insight into the understanding of the various interaction sin this dimeric lattice and to evaluate the **g** and **A** tensor values, we undertook a study of the pure single crystal of $(n\text{-}Bu_4N)_2{}^{63}Cu(dcmdtcroc)_2$ using EPR at Q-band fields. The single-crystal spectra were followed by scanning the magnetic field in the three crystallographic planes (*ab*, *bc*, and *ac*) identified from the external morphology of the crystal shown in Figure 10. All three planes showed the presence of two magnetically inequivalent sites except when $\vec{B}$ is parallel to one of the crystallographic axes, as expected from the crystallographic packing (Figure 3). However, besides the two sets of lines expected for the two sites, a number of other lines, smaller in intensity, was seen to vary with the temperature (Figure 11). This proves the existence of interdimer interaction in this system as already suggested by the susceptibility measurements.

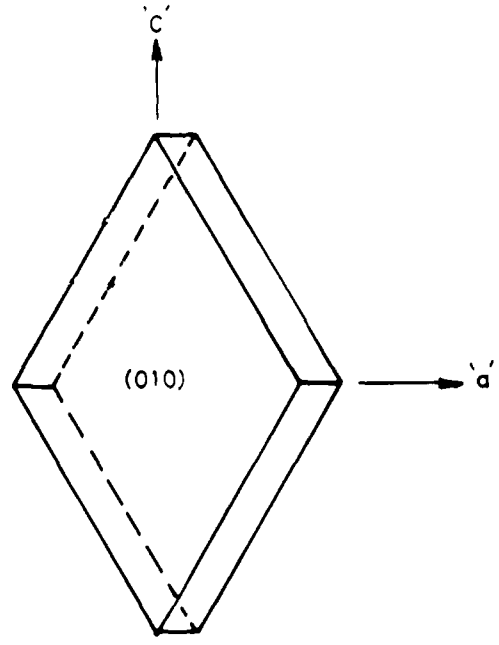

Figure 10. Morphology of a single crystal of $(n\text{-}Bu_4N)_2Cu(dcmdtcroc)_2$.

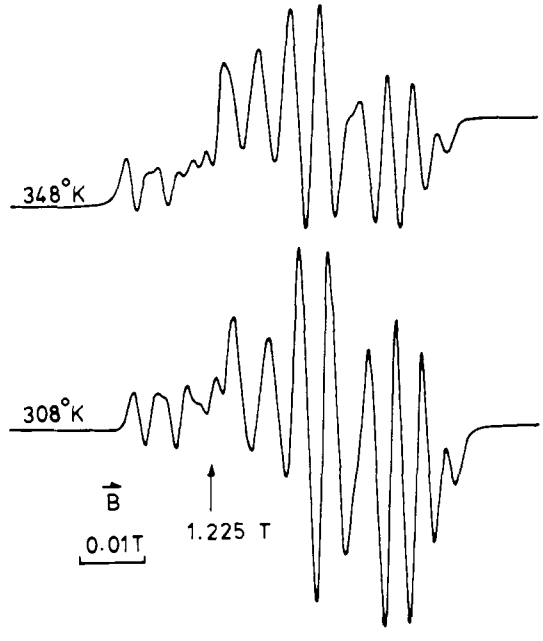

Figure 11. Temperature-dependent Q-band EPR spectra of a single crystal of $(n\text{-}Bu_4N)_2Cu(dcmdtcroc)_2$ in an arbitrary orientation in the *ac* plane.

At least an explanation as to the origin of such temperature-dependent low-intensity lines is essential at this stage, although this has been explained in the work of Snaathorst et al.[10] The isolated triplet (T) and pair triplet (T_p) states shown in Figure 9D are pure states independent of the magnitude of J_{inter}. All large intensity lines seen in most of the orientations are due to the overlap of T and T_p levels. One of the important characteristics of T and T_p states is that they do not shift upon changing the magnitude of J_{inter}. However, out of the six $\Delta M_s = 1$ transitions allowed within the mixed S–Q manifold of the TT state, two of

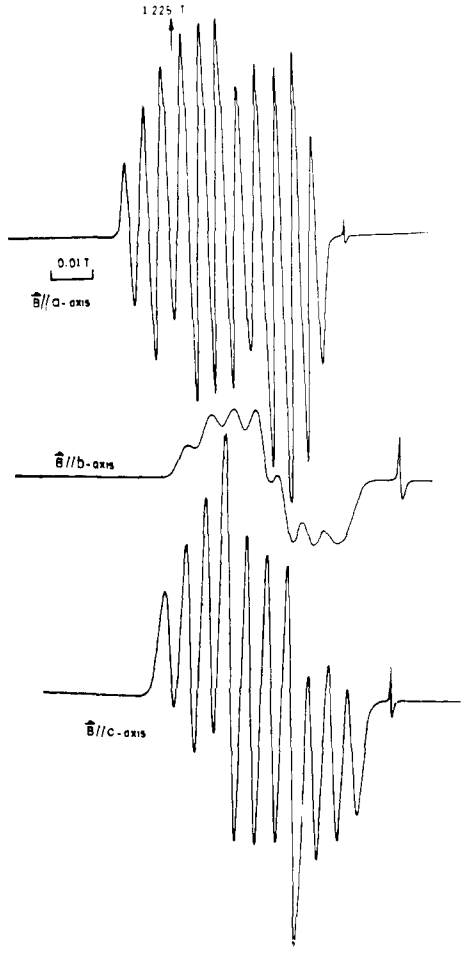

Figure 12. Q-band EPR spectra of a single crystal of $(n\text{-}Bu_4N)_2$ Cu(dcmdtcroc)$_2$ along the three crystallographic axes.

them (Q) are independent of J_{inter} and the other four (SQ and QS) strongly depend on the magnitude and sign of J_{inter}. Especially the intensities of SQ transitions are inversely proportional to the value of $|J_{inter}|$. It is possible that some of these small intensity lines originate from these states. It is justified by the fact that such lines in a particular orientation (Figure 11) decrease in intensity as temperature is increased due to the depletion of TT states responsible for such transitions. It would be ideal to prove their total absence at a higher temperature, but unfortunately the crystals tend to decompose at such temperatures. The magnitude of J_{inter} as calculated from molecular field calculation, viz. -0.041 cm^{-1}, could have caused these intensities. The evaluation of **g** and **A** tensors by a simple diagonzalization procedure is not possible in this case. However, the EPR spectra when $\vec{B}$ is parallel to *a*, *b*, and *c* crystallographic axes are relatively simple as shown in Figure 12 because of the equivalence of the two sites. When $\vec{B}||a$ and $\vec{B}||c$, two sets of seven lines separated by **D** value are observed, and when $\vec{B}||b$ only one set of seven lines are obtained indicating that it is the turnover point in the zero-field splitting $\vec{B}$ vs angle plot. This permits a reasonably accurate estimate of the spin Hamiltonian parameters possible using the simplified Hamiltonian

$$\mathcal{H} = \beta\vec{B}\cdot\mathbf{g}\cdot\vec{S} + \vec{S}\cdot D\cdot\vec{S} + \vec{I}\cdot A\cdot\vec{S} \qquad (14)$$

The **D** value has also been arrived at from the polycrystalline spectra. Using these rough values of spin Hamiltonian parameters and the direction cosines calculated from the crystal structure with the tensor directions originating from the center of Cu–Cu axis, the EPR spectra can be simulated by using the computer program MAGNSPEC[18] devloped by Knopp and Mackey. We have also

(18) (a) Mackey, M. H.; Kopp, M.; Tynan, E. C.; Yen, T. F. *Electron Spin Resonance of Metal Complexes*; Yen, T. F., Ed.; Plenum: New York, 1969. (b) Kopp, M.; Mackey, J. H. *J. Com. Phys.* **1969**, *3*, 539-557.

Table V. Spin Hamiltonian Parameters

spin parameters	from single-crystal EPR	from polycrystalline EPR
$\mathbf{g}_{xx}$	2.026	2.03
$\mathbf{g}_{yy}$	2.033	2.03
$\mathbf{g}_{zz}$	2.097	2.09
$\mathbf{A}_{xx}$	34.3×10^{-4} cm^{-1}	30.0×10^{-4} cm^{-1}
$\mathbf{A}_{yy}$	37.2×10^{-4} cm^{-1}	30.0×10^{-4} cm^{-1}
$\mathbf{A}_{zz}$	118.6×10^{-4} cm^{-1}	120.0×10^{-4} cm^{-1}
D	102×10^{-4} cm^{-1}	
J		12.0 cm^{-1}

assumed the coincidence of **g**, **A**, and **D** tensors. Table V gives the spin Hamiltonian parameters which give the best fit with the experimental curves. However, a more detailed analysis inclusive of all orientations will be reported later. It is true, that we have not included the $JS_1\cdot S_2$ term in interpretation of the single-crystal spectrum, while we have included the same in polycrystalline EPR spectra interpretation. It is, hence, expected that the values of **g**, **A**, and **D** may not be very accurate. This is evident from Table V containing the EPR spin Hamiltonian parameters.

(vi) **Bonding.** It is necessary at this point to comment and compare the magnetic properties of the three well-established exchange-coupled dimers of the copper(II) dithiolenes where the CuS_4 unit is not planar. Unlike most other exchange-coupled systems, here the exchange interaction is of intermolecular origin. A simple EHT calculation performed on planar and bent Cu(mnt)$_2^{2-}$ as a function of the dihedral angle between the two chelate planes reveals the following: (i) a progressive decrease in the metal d_{xy} character in the MO of the unpaired electron on increasing the dihedral angle; (ii) a progressive increase in the metal $4p_z$ character of metal in this MO until the dihedral angle reaches 45°; (iii) the presence of p_z character of sulfur and carbon in this MO on increasing the dihedral angle; and (iv) a decrease in the self-consistent charge on the metal. However, a calculation on Cu(dcmdtcroc)$_2^{2-}$ indicates that the trends monitored above are broken mainly because of the extensive delocalization on the ligand. This is borne out later by a comparison of the ESR results.

Some of these calculated values are given especially for the dihedral angles corresponding to the nonplanar complex ions in Table VI along with magnetic and relevant crystallographic information. First it is obvious that the exchange interaction is facilitated by the nearness of the two interacting metal centers {as in $(n\text{-}Bu_4N)_2$Cu(dcmdtcroc)$_2$} or by the close interplanar spacing between two different molecules {$(MB^+)_2$Cu(mnt)$_2$}. The $4p_z$ characters of the metal and ligand sulfur and carbon atoms in the MO containing the unpaired electron greatly enhances the overlap between the centers of the first molecule and the appropriate centers of the second molecule giving rise to a superexchange pathway. In $(NMe_4)_2$Cu(mnt)$_2$, not only the Cu–Cu distance is large but also the interplanar distance between the two S_1–Cu–S_2 moieties, making it least susceptible to exchange interaction. The exchange interaction in this system was found to be of the order of a few hundredth of a cm^{-1} as determined by EPR line width analysis.[19] However, in $(n\text{-}Bu_4N)_2$Cu(dcmdtcroc)$_2$, though the two planes of ligands within the dimeric unit related by a center of symmetry are pulled by a slip along the *y*-coordinate of a single complex ion, a short intercopper distance of 4.88 Å allows Cu–Cu′ (unprimed atom representing one center and primed one the other center of the exchange coupled dimer) to interact heavily through the 3s and 3p orbitals of S_3 and S_3' of the dithiolenes, the minimum overlap values between the metal p_z orbitals and the sulfur orbitals being about 0.1. In the case of $(MB^+)_2$Cu(mnt)$_2$, though the Cu–Cu′ distance is as high as 7.11 Å because of a considerable slip of copper along the *y*-direction of the complex ion, a very short interplanar separation of only 3.1 Å facilitates an effective overlap between Cu–S_2–C_2–C_6 and C_6'–C_2'–S_2'–Cu′ centers, the overlaps between the concerned orbitals of the appropriate centers being in the region of 0.065–0.160. Hence it is not surprising to see

(19) Kuppusamy, P.; Manoharan, P. T. *Inorg. Chem.* **1985**, *24*, 3053-3060.

Table VI. Comparison of Salient Features in the Nonplanar Dithiolenes[a]

	A	B (B′)[b]	C	D
crystallographic data				
dihedral angle (deg)	0.0	36.76	41.14	47.4
Cu–Cu dist in dimer (Å)	9.403	4.880	7.810	7.110
interplanar dist in dimer (Å)	6.91	4.49	7.56	3.10
projd Cu–Cu dist along X-axis (Å)	0.61	0.13	0.32	0.86
projd Cu–Cu dist along Y-axis (Å)	6.34	1.90	1.93	6.35
magnetic data				
$2J$ (cm^{-1})	0.021	12.0	0.0	−5.2
MO calcd				
charge	0.12	0.04 (0.084)	0.08	0.07
Cu p_z	0	0.0402 (0.025)	0.026	0.026
Cu d_{xy}	0.265	0.204 (0.245)	0.2433	0.2389
unpaired electron density				
S p_x	0.126	0.0747 (0.098)	0.0938	0.087
S p_y	0.0368	0.018 (0.02)	0.0175	0.0129
S p_z	0	0.006 (0.04)	0.0457	0.0559
ref c	5	this work	10	9

[a] A = $(n\text{-}Bu_4N)_2Cu(mnt)_2$, B = $(n\text{-}Bu_4N)_2Cu(dcmdtcroc)_2$, C = $(Me_4N)_2Cu(mnt)_2$, D = $(MB^+)_2Cu(mnt)_2$. [b] MO calcd on the hypothetical B′ = $Cu(mnt)_2^{2-}$ with a dihedral angle of 36.76 are quoted in brackets. [c] The crystallographic and the magnetic data alone are taken from other references. MO information for all complexes are from this work.

that the magnitude of exchange interaction in these two cases is large when compared to the almost noninteracting complex ions in $(NMe_4)_2Cu(mnt)_2$. The intermolecular dimeric structures in these three systems are presented in Figure 13 with a view to emphasize the highly overlapping centers. At least, it is possible to guess from this figure that the orbitals from centers of the individual monomers of $(NMe_4)_2Cu(mnt)_2$ are so far apart making them impossible to overlap revealing an extremely low exchange coupling constant. In the other two molecules, the overlapping centers are in reasonably close proximity to permit overlap though of smaller magnitude and hence musch higher exchange coupling constants for them. However, what is not apparent now is not only the change in sign of the exchange interaction of these two molecules but also the differences in the magnitude of $2J$. It is possible that the contributions from ferromagnetic and antiferromagnetic components as suggested by Kahn[20] must be different for these systems possibly because of the differences in the nature and magnitudes of overlap. The theoretical calculations of exchange couplings are under further investigation.

The planar dithiolene moiety has a D_{2h} symmetry. However, the symmetry is reduced to D_2 when nonplanarity sets in. The molecular orbital of the unpaired electron of the planar molecule consists of the $3d_{xy}$ of copper and the corresponding symmetry-adapted LCAO's from the 3s, $3p_x$, and $3p_y$ orbitals of sulfur atoms. On twisting the ligands, the molecular orbital of the unpaired electron is a mixture of $3d_{xy}$ and $4p_z$ orbitals of copper and has also p_z character for the ligand component as revealed by the MO calculation. This mixing has a direct effect on copper hyperfine splitting as shown by Keijzers and de Boer[21] and recently by Snaathorst et al.[10] They have shown that the coefficients of the $3d_{xy}$ and $4p_z$ of copper in this MO, say α and β, respectively, could be combined together to get a first-order hyperfine splitting due to the spin densities in these orbitals:

$$A(3d_{xy}):A(4p_z) = -5\alpha^2\langle r^{-3}\rangle_{3d}:7\beta^2\langle r^{-3}\rangle_{4p} - 2\alpha^2:\beta^2$$

This equality takes into consideration the differences in the values of $\langle r^{-3}\rangle_{3d}$ and $\langle r^{-3}\rangle_{4p}$ as calculated from the atomic wave functions.[21] We have, therefore, correlated the sum of MO contribution $(-2\alpha^2 + \beta^2)$ with the anisotropic component $(A'_{\parallel} = A_{\parallel} - A_{av})$ of the hyperfine part from the experrmental values. This is shown in Figure 14. Though there are only three points in the linear plot, it is included only to indicate the importance of the delocalization and twist effects in deciding the resultant contribution to the first-order hyperfines due to $^{63,65}Cu$. While it is true that the twisting effect simply redistributes the unpaired electron densities in the $3d_{xy}$ and $4p_z$ orbitals keeping the same total unpaired density on the metal atom {as shown by $Cu(mnt)_2^{2-}$ with different twist angles}, one has to consider in $Cu(dcmdtcroc)_2^{2-}$ not only the twist effects but also the greater delocalization effect.

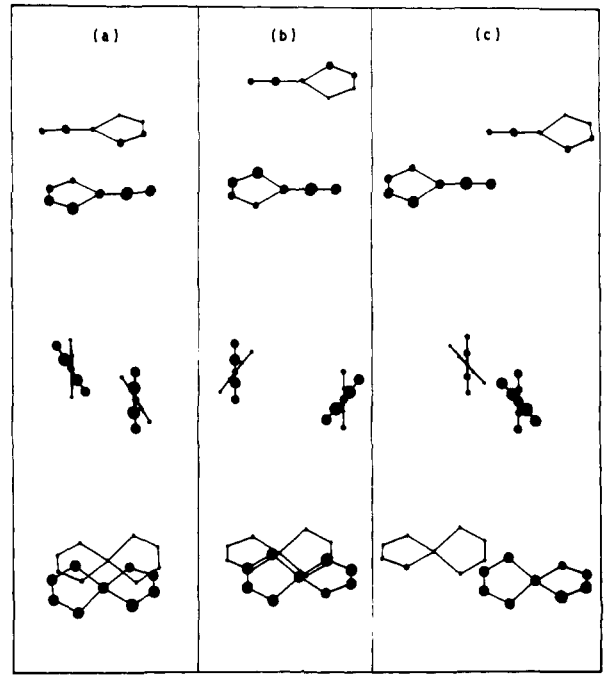

Figure 13. A view of the intermolecular dimeric structures in (a) $(n\text{-}Bu_4N)_2Cu(dcmdtcroc)_2$, (b) $(NMe_4)_2Cu(mnt)_2$, and (c) $(MB^+)_2Cu(mnt)_2$. Projection perpendicular to one of the Cu–S–C–C–S planes (bottom), perpendicular to the bisector of S–Cu–S angle (middle), and parallel to it in the plane shown at bottom (top).

A comment on the value of **D** may be appropriate here. Total contribution to the observed **D** comes from $\mathbf{D}^{dip}$ and $\mathbf{D}^{ex}$. The $\mathbf{D}^{dip}$

(20) Kahn, O.; Charlot, M. F. *Nouv. J. Chem.* **1980**, *5*, 567.
(21) Keijzers, C. P.; de Boer, E. *J. Chem. Phys.* **1972**, *57*, 1277.

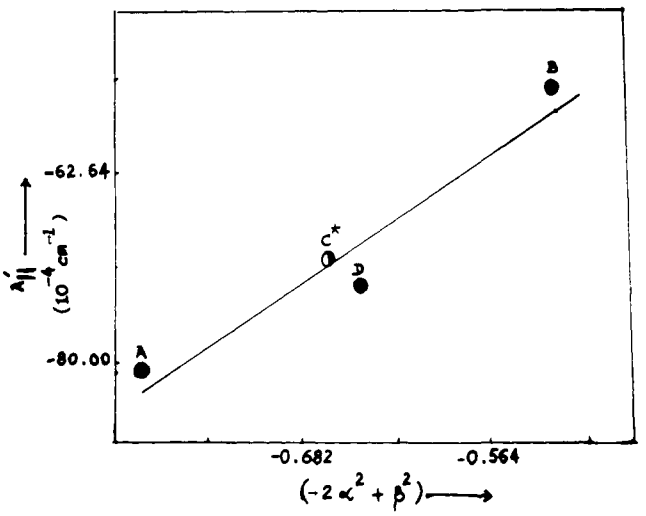

Figure 14. A correlation of experimental anisotropic hyperfine splitting due to $^{63,65}Cu$ ($A_{\parallel} = A - A_{av}$) and calculated molecular orbital coefficients from $3d_{xy}$ and $4p_z$ of Cu: A = planar $(n\text{-}Bu_4N)_2Cu(mnt)_2$; B = bent $(n\text{-}Bu_4N)_2Cu(dcmdtcroc)_2$; C = bent $(Me_4N)_2Cu(mnt)_2$; (* indicates unavailability of experimental data on $A'_{\parallel}$); D = $(MB^+)_2Cu(mnt)_2$.

as calculated from point charge model yields 168 G with the observed Cu-Cu bond distance in the dimeric unit. However, it is expected to decrease with increased covalency. Hence, the estimated D^{dip} term will only be about 80-90 G in this complex. Furthermore, D^{ex} can be calculated by the equation[23]

$$D^{ex} = \tfrac{1}{8}(2J)\,[0.25(g_{zz} - 2.0023)^2 - 0.5\{(g_{xx} - 2.0023)^2 + (g_{yy} - 2.0023)^2\}] \quad (15)$$

and it turns out to be 28 G with the observed $2J$ of 12 cm^{-1}. The total observed **D** of 102 G at room temperature compares very favorably with the calculated value of about 108-118 G though the model may be simple.

Conclusion

The lattice of $(n\text{-}Bu_4)_2Cu(dcmdtcroc)_2$ is an interesting example of ferromagnetically coupled dimer with an antiferromagnetic interdimer coupling. The $2J$ value calculated from susceptibility, powder simulations of EPR using an appropriate Hamiltonian, and temperature variation of intensity all lead to an identical conclusion revealing an interesting method of deriving $2J$. The interdimer coupling and its manifestations on EPR spectra are not correctly identifiable at this stage.

Acknowledgment. We thank Professor John R. Pilbrow and S. R. Sinclain of Monash University, Australia for providing their EPR powder simulation program used in this paper. N.V.L. is grateful to the Council of Scientific and Industrial Research, India for providing a fellowship and B.V. to the DST, Government of India, for a research associateship. This work was supported by a scheme from the Department of Science and Technology, Government in India. Thanks are also due to the Regional Sophisticated Instrumentation Centre, Madras, India for providing instrumental facilities.

Supplementary Material Available: Tables containing the anisotropic temperature factors for the non-hydrogen atoms and the positional parameters for the hydrogen atoms (4 pages); table of observed and calculated structure factors for $(n\text{-}Bu_4)_2[Cu(dcmdtcroc)_2]$ (20 pages). Ordering information is given on any current masthead page.

(22) Bancroft, G. M. *Mossbauer Spectroscopy*; McGraw-Hill: London, 1973; p 27.
(23) Bleaney, B.; Bowers, K. D. *Proc. Roy. Soc., Ser. A* **1952**, *214*, 451.

X-ray Crystal Structure of $ReH_5(PPh_3)_3$ and Variable-Temperature T_1 Studies on $ReH_5(PPh_3)_3$ and $ReH_5(PMe_2Ph)_3$ in Various Solvents: Are T_1 Measurements Reliable in Predicting Whether Polyhydride Complexes Contain Molecular Hydrogen Ligands?

F. Albert Cotton* and Rudy L. Luck

Contribution from the Department of Chemistry and Laboratory for Molecular Structure and Bonding, Texas A&M University, College Station, Texas 77843. *Received December 7, 1988*

Abstract: The variable-temperature ^1H NMR longitudinal relaxation times (T_1) and spectra of the complexes $ReH_5(PPh_3)_3$ in toluene-d_8 and CD_2Cl_2 and $ReH_5(PMe_2Ph)_3$ in CD_2Cl_2 are reported. The trends observed are in keeping with our previous assignment of $ReH_5(PPh_3)_3$ as containing a dihydrogen (η^2-H_2) ligand. However, the X-ray structure determination of this complex reveals no bonding H-H interactions and gives an average Re-H distance of 1.54 [5] Å. Crystal data for $ReH_5(PPh_3)_3$: monoclinic, space group $P2_1/n$, a = 9.968 (4) Å, b = 33.237 (9) Å, c = 13.591 (4) Å, β = 92.27 (3)°, V = 4500 (3) Å^3, Z = 4, R = 0.0376 (R_w = 0.0482) for 436 parameters and 4824 unique data having $F_o^2 > 3\sigma(F_o)^2$.

There has been renewed interest in the properties of rhenium polyhydride complexes[1] especially as to whether these complexes contain molecular hydrogen (η^2-H_2) ligands.[2-5] In a recent communication[2b] we pointed out that the classical formulation of $ReH_5(PPh_3)_3$,[5] **1**, based on a reported T_1 value of 540 ms, was incorrect. Our conclusion was based on the fact that we obtained much lower T_1 values than reported earlier for **1** (T_1 (min) = 46

(1) Conner, K. A.; Walton, R. A. in *Comprehensive Coordination Chemistry*; Pergamon: Oxford, England, 1987; Chapter 43, pp 125-213.
(2) (a) Cotton, F. A.; Luck, R. L. *J. Chem. Soc., Chem. Commun.* **1988**, *19*, 1277. (b) Cotton, F. A.; Luck, R. L. *Inorg. Chem.* **1989**, *28*, 6. (c) Cotton, F. A.; Luck, R. L. *Inorg. Chem.* **1989**, *28*, 2181.
(3) Costello, M. T.; Walton, R. A. *Inorg. Chem.* **1988**, *27*, 2563.
(4) Fontaine, X. L. R.; Fowles, E. H.; Shaw, B. L. *J. Chem. Soc., Chem. Commun.* **1988**, 482.
(5) (a) Hamilton, D. C.; Crabtree, R. H. *J. Am. Chem. Soc.* **1988**, *110*, 4126. (b) Crabtree, R. H.; Hamilton, D. G. *Adv. Organometallic Chem.* **1988**, *28*, 299.

0002-7863/89/1511-5757$01.50/0